The Journal of Chemical Physics

RESEARCH ARTICLE | APRIL 22 2026

Pressure induced structural transition and optoelectronic modification in inorganic metavanadate phosphor

Zhenfang Xing ; Yuntao Jie; Yuqi Sun ; Xingxing Zhao ; Di Peng; Songhao Guo ; Yifan Zhang ; Congcong Chen; Tongge Xu; Ziyao Liu; Gui Wang; Xujie Lü ; Zhidan Zeng ; Yonghao Han ; Lin Zhao ; Meiling Xu ; Qiaoshi Zeng

J. Chem. Phys. 164, 164701 (2026)
https://doi.org/10.1063/5.0317089

AIP Publishing

The Journal of Chemical Physics ARTICLE pubs.aip.org/aip/jcp

Pressure induced structural transition and optoelectronic modification in inorganic metavanadate phosphor

Cite as: J. Chem. Phys. 164, 164701 (2026); doi: 10.1063/5.0317089
Submitted: 16 December 2025 • Accepted: 6 April 2026 •
Published Online: 22 April 2026

Zhenfang Xing,[1,2] Yuntao Jie,[3] Yuqi Sun,[1] Xingxing Zhao,[4] Di Peng,[5] Songhao Guo,[2] Yifan Zhang,[2] Congcong Chen,[2] Tongge Xu,[1] Ziyao Liu,[1] Gui Wang,[2] Xujie Lü,[2] Zhidan Zeng,[2] Yonghao Han,[1] Lin Zhao,[1,a)] Meiling Xu,[3,a)] and Qiaoshi Zeng[2,5,a)]

AFFILIATIONS

[1] State Key Laboratory of High Pressure and Superhard Materials, College of Physics, Jilin University, Changchun 130012, China
[2] Center for High Pressure Science and Technology Advanced Research, Shanghai 201203, China
[3] Laboratory of Quantum Functional Materials Design and Application, School of Physics and Electronic Engineering, Jiangsu Normal University, Xuzhou 221116, China
[4] College of Physics and Optoelectronic Engineering, Shenzhen University, Shenzhen 518060, China
[5] Shanghai Key Laboratory of Material Frontiers Research in Extreme Environments (MFree), Shanghai Advanced Research in Physical Sciences (SHARPS), Shanghai 201203, China

[a)] **Authors to whom correspondence should be addressed:** zhaolin@jlu.edu.cn; xml@calypso.cn; and zengqs@hpstar.ac.cn

ABSTRACT

AVO_3 metavanadates (A: alkali metal) have been reported as promising inorganic white-light-emitting phosphors due to their self-activated broadband luminescence caused by the charge transfer transition in the VO_4 tetrahedra. In particular, $CsVO_3$ attracts much attention due to its highest quantum efficiency. Here, the optical and structural properties of $CsVO_3$ are investigated under high pressure by a combination of theoretical and experimental studies. A pressure-induced structural transition from the orthorhombic to monoclinic phase is found by crystal structure prediction and further verified by x-ray diffraction and Raman spectroscopy measurements. The structural transition is accompanied by the distortion and reorientation of VO_4 tetrahedra, resulting in an ultrabroad emission tunability both in peak position (from 542 to 672 nm) and full-width at half-maximum (from 158 to 194 nm) and, therefore, making $CsVO_3$ present a white-light emission tendency after pressurization. Moreover, absorption spectra and first-principles calculations reveal a direct-indirect bandgap transition at ~12 GPa, corresponding to the structural phase transition. These results provide new insights into the structural and optical modulation of metavanadate phosphor and promote the development of inorganic solid luminescent materials under pressure.

I. INTRODUCTION

Alkali metal metavanadates AVO_3 (A = K, Rb, Cs) have been reported as promising white-light-emitting phosphors due to their self-activated broadband luminescence and good color rendering performance. Compared to the conventional rare earth phosphors and metal halide perovskites, metavanadates have the advantages of good chemical stability, low fabrication temperature, and low cost, making them attractive for solid-state lighting and display applications.[1–14] In particular, $CsVO_3$ has attracted much attention due to its high internal quantum efficiency and wide tunability of emission spectra ranging from 400 to 800 nm.[15–17] At ambient conditions, $CsVO_3$ has an orthorhombic structure with Pbcm symmetry and consists of VO_4 tetrahedral chains linked by V–O–V bonds. According to the molecular orbital theory, the luminescence of $CsVO_3$ originates from the charge transfer transition of an electron from the O 2*p* to the V 3*d* orbital in the VO_4 tetrahedra with Td symmetry.[18–24] Therefore, the VO_4 tetrahedra distortion through

structural modulation could significantly affect the optoelectronic properties of $CsVO_3$.

Pressure, as a fundamental thermodynamic parameter, provides a powerful pathway to modulate the lattice symmetry and electronic orbitals of materials by altering their crystal and electronic structure.[25–27] In earlier reports, Adams *et al.* studied the structure stability of $CsVO_3$ at high pressure by synchrotron x-ray powder diffraction measurements up to 10 GPa; they found that $CsVO_3$ shows no phase transition below 10 GPa.[28] Meanwhile, Kourouklis *et al.* have reported that $CsVO_3$ undergoes structural phase transitions above 10 GPa by Raman spectroscopy measurements.[29] They suggested that the structural transition is associated with the rotations and distortions of the corner sharing tetrahedral chains, but the high-pressure crystal structure of $CsVO_3$ was not resolved. In addition, there were no further experimental studies on $CsVO_3$ under pressure, and the relevant theoretical studies were also limited to the ambient phase of $CsVO_3$.[30–32] Since the luminescent properties of $CsVO_3$ are closely related to the VO_4 tetrahedra structures, it is necessary to investigate in depth the structural phase conversion as well as its impact on the optoelectronic behavior of $CsVO_3$ under pressure. While previous studies suggested a phase transition, the crystal structure and its consequent impact on optoelectronic properties remained unknown.

Here, we carried out a systematic high-pressure study on $CsVO_3$ under a wide pressure range of 0–20 GPa. Combining *in situ* x-ray diffraction, Raman spectroscopy measurements, and *ab initio* calculations, we identify a monoclinic *Pc* phase of $CsVO_3$ above ~12 GPa. This monoclinic phase is transformed from the ambient orthorhombic phase via the rearrangement and reconstruction of the VO_4 tetrahedra. High-pressure photoluminescence (PL) measurements show an ultrabroad emission tunability both in peak position (from 542 to 672 nm) and full-width at half-maximum (FWHM) (from 158 to 194 nm), corresponding to the structural transition process. Absorption spectra and first-principles calculations reveal that $CsVO_3$ also undergoes a direct-indirect bandgap transition from the *Pbcm* to the *Pc* phase. These results gain a deep understanding about the structural and optical properties of $CsVO_3$ under pressure and provide insights into the application of metavanadate phosphor at extreme conditions.

II. METHODS

A. High pressure generation

High-pressure experiments were conducted in symmetric DAC devices. A pair of type II-a ultra-low fluorescence diamond anvils with a culet diameter of 300 μm was employed to generate high pressure and prevent the influence of the diamond optical signal. The sample chamber with a diameter of ~100 μm and a thickness of ~35 μm was drilled from a T301 steel gasket. The polycrystalline $CsVO_3$ was loaded into the sample chamber together with a small ruby, and the pressure was determined by the ruby fluorescence method.[33] All experiments were performed at room temperature.

B. X-ray diffraction (XRD) experiments

In situ high-pressure x-ray diffraction (XRD) experiments were conducted at room temperature using a liquid metal x-ray diffraction instrument with a wavelength of 0.5124 Å. The instrument parameters were calibrated with a CeO_2 standard sample. The integration of the two-dimensional XRD patterns was processed using the DIOPTAS program.[34] Rietveld refinement of the XRD patterns was performed using FullProf software.[35]

C. Raman scattering experiments

Raman spectroscopy measurements were performed at room temperature using a Princeton Instruments Acton SP2500. A laser with a wavelength of 488 nm and an intensity of 10 mW was used as the excitation light source. A 20× long-working-distance objective and a 1200 g mm^{-1} grating were used to collect and disperse the Raman signals. The spectral data recording time was 30 s, and a 1024-pixel charge-coupled device (CCD) developed by Princeton was employed. The diameter of the laser spot for Raman measurements was ~10 μm.

D. Photoluminescence measurements

The *in situ* high-pressure PL spectra were recorded by a home-designed spectroscopy (Gora-UVN-FL, Ideaoptics, Shanghai, China) with an excitation wavelength of 360 nm. An anomalous fluctuation at 556 nm in the raw data was attributed to instrumental factors. During data processing, normalization was achieved by subtracting the background and dividing the results by the maximum intensity value at ambient pressure.

E. UV–vis absorption measurements

In situ high-pressure optical measurements were performed using a UV–Vis absorption spectrometer with an exposure time of 1.2 s at room temperature. The UV–Vis system consists of a deuterium lamp, a halogen lamp, an absorption optical system, and a CCD detector. The collected wavelength range is 250–850 nm. The background signals were collected from the regions without a sample using the same measurement parameters.

F. Crystal structure prediction

The particle swarm optimization (PSO) method within the evolutionary algorithm, as implemented in the Crystal structure AnaLYsis by Particle Swarm Optimization (CALYPSO) code,[36–40] was employed to search for the lowest-energy structures of $CsVO_3$. Unit cells containing 1–4 formula units (f.u.) were considered. In the initial step, random structures with specified symmetries were generated, with atomic coordinates determined by crystallographic symmetry operations. Local structural optimizations were performed using the Vienna *ab initio* Simulation Package (VASP) code with the conjugate gradient method and were terminated when the change in Gibbs free energy fell below 1×10^{-5} eV per cell. After evaluating the first generation, 60% of the structures with the lowest Gibbs free energies were selected to produce the next generation via PSO, while the remaining 40% were randomly generated to maintain structural diversity. A structure fingerprinting technique based on a bond characterization matrix was applied to eliminate duplicates, ensuring that identical structures were strictly excluded. This approach greatly enhances structural diversity, which is critical for the efficiency of global structure searches.

G. First-principles calculations

Structural relaxations and electronic structure calculations were performed within the framework of density functional theory (DFT),[41] as implemented in the VASP.[42,43] The exchange–correlation interactions were treated using the Local-Density-Approximation (LDA),[44] and the projector augmented-wave (PAW) method[45] was employed to describe the electron–ion interactions. The valence electrons included in the calculations were Cs ($5s^2 5p^6 6s^1$), V ($2p^6 3d^4 4s^1$), and O ($2s^2 2p^4$). A plane-wave cutoff energy of 600 eV was used for all calculations. The Brillouin zone was sampled using Monkhorst–Pack[46] k-point grids of 9 × 4 × 8 and 10 × 7 × 13 for the *Pbcm* and *Pc* phases, respectively. Structural optimizations were performed until the total energy and atomic forces converged to within 10^{-7} eV and 0.001 eV/Å, respectively. Phonon dispersion relations were computed using the finite-displacement method with a 2 × 2 × 3 supercell, as implemented in the PHONOPY package.[47]

III. RESULTS AND DISCUSSION

A. High-pressure structure prediction of $CsVO_3$ using CALYPSO method

We first clarify the structural phase transition of $CsVO_3$ under pressure. In order to determine the high-pressure structure, we have performed crystal structure prediction by using CALYPSO in the pressure range of 0–20 GPa. The calculations indicate that the most stable structure above 12.0 GPa is a monoclinic structure with *Pc* (No. 7) symmetry, and the relative enthalpy between the *Pc* phase and the *Pbcm* phase is shown in Fig. 1(e). The underlying structural transition process can be understood through the crystal structure diagrams of $CsVO_3$ in different phases, as shown in Figs. 1(a)–1(d). From the *Pbcm* phase toward the *Pc* phase, the angle between two adjacent VO_4 tetrahedra significantly decreases, resulting in a drastic twisting of the tetrahedral chain [Figs. 1(a) and 1(b)]. Meanwhile, the tetrahedra are deformed due to the symmetry conversion, lengthening certain V–O bonds toward an asymmetric tetrahedral structure [Figs. 1(c) and 1(d)]. As a result, the new monoclinic *Pc* phase is achieved via the rearrangement and reconstruction of the VO_4 tetrahedra. To confirm the dynamical stability of the predicted structure, we also calculated the phonon band and partial density of states (PDOS) in *Pc* symmetry at 16 GPa. The absence of imaginary frequencies indicates that the *Pc* phase is dynamically stable under high pressure [Fig. 1(f)].

B. High-pressure structure verification by XRD and Raman spectroscopy

To verify the structural phase transition in experiments, we conducted high-pressure *in situ* XRD measurements on $CsVO_3$ via a diamond anvil cell up to 20 GPa. Figure 2(a) shows the powder diffraction patterns under various pressures. At ambient pressure, all the diffraction peaks can be indexed to the orthorhombic *Pbcm* structure [Fig. 2(b)]. With increasing pressure to 12.5 GPa, obvious changes are observed in the XRD patterns as two initial peaks at 7°–8° disappeared and a new notable diffraction peak appeared at ~11°, suggesting that a new high-pressure phase was produced. One can notice that the high-pressure phase has showed a slight sign at ~6 GPa, marked by the left shoulder of the initial peak at 11.3°, but its proportion is too small to be identified from the ambient XRD patterns. As the pressure increased, the shoulder peak gradually strengthened and shifted toward lower angles, eventually becoming a new prominent peak at 12.5 GPa. Meanwhile, another new diffraction peak emerged around 12° and gradually shifted to higher angles above 12.5 GPa. Therefore, we consider the phase transition pressure to be 12.5 GPa thereafter. Note that the calculated enthalpy crossing predicts the phase transition at 12.0 GPa, while our experimental observations become unequivocal at 12.5 GPa. This slight discrepancy is common and can be attributed to the experimental pressure gradient. Based on our predicted monoclinic *Pc* structure at high pressure, we further performed Rietveld refinements on the experimental XRD data at 15.7 GPa. As shown in Fig. 2(b), the experimental and calculated XRD patterns are in good agreement, which confirms the reliability of the predicted structure. The

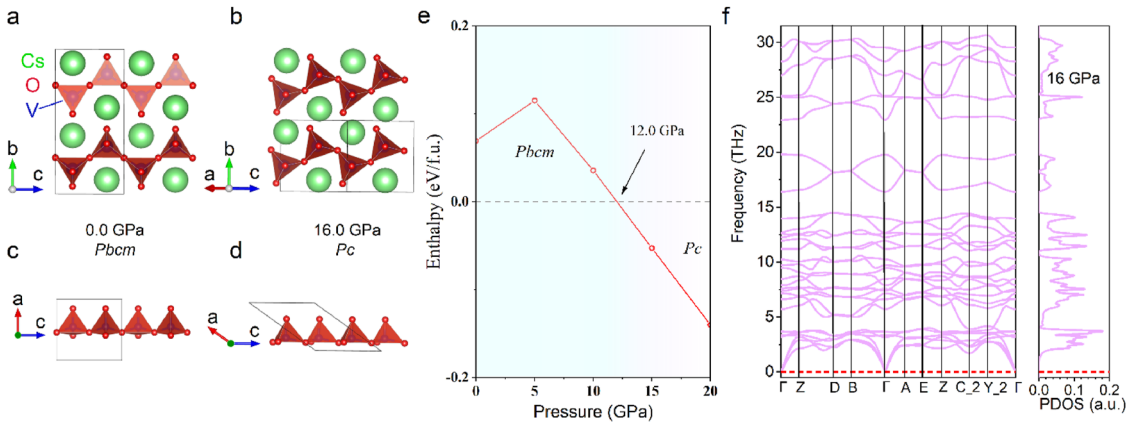

FIG. 1. Crystal structures of $CsVO_3$ in (a) *Pbcm* phase at 0 GPa and (b) *Pc* phase at 16 GPa. Polyhedral views of the VO_4 tetrahedra in the (c) *Pbcm* and (d) *Pc* phases. (e) Relative enthalpy between the *Pbcm* and *Pc* phases as a function of pressure: the enthalpy of the *Pbcm* phase is set as the basis. (f) Phonon band and partial density of states (PDOS) for the *Pc* phase at 16 GPa.

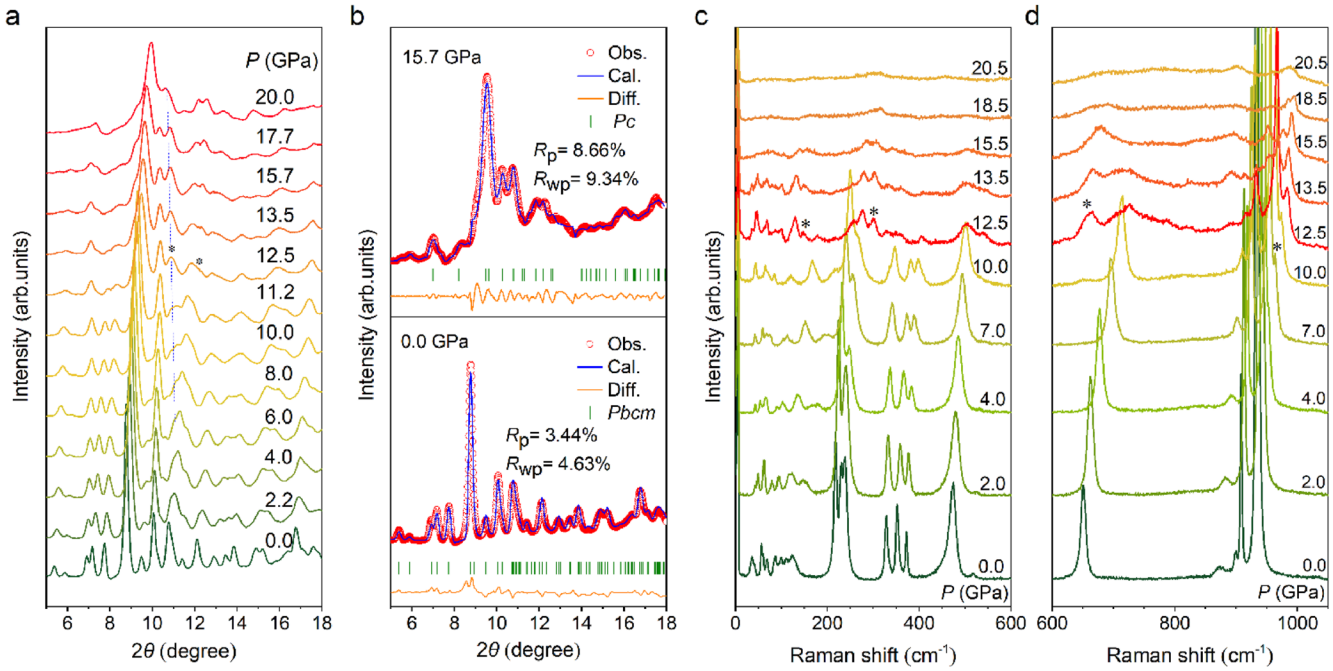

FIG. 2. Characterization of structural phase transition under high pressure. (a) XRD patterns of $CsVO_3$ under various pressures. The x-ray wavelength λ = 0.5124 Å. (b) Rietveld refinements of the XRD patterns at 0 and 15.7 GPa by using *Pbcm* and *Pc* structures. (c) and (d) Raman spectra of $CsVO_3$ under various pressures up to 20.5 GPa. The * symbol denotes new peak formation.

experimental and calculated lattice parameters for both the *Pbcm* and *Pc* phases are listed in Table I (details on atomic coordinates are given in Table S1), compared to available experimental data.[14,48]

In order to gain a deeper understanding of the structural evolution and lattice dynamics of $CsVO_3$ under high pressure, *in situ* Raman spectroscopy measurements were also conducted. Figures 2(c) and 2(d) present the Raman spectra of $CsVO_3$ under various pressures up to 20.5 GPa. At ambient conditions, 23 Raman modes are detected in the frequency range of 0–1100 cm^{-1}, consistent with the reported Raman data.[49] According to the previous group analysis, the ambient Raman modes can be divided into five different types of vibrational modes. The modes at 0–200 cm^{-1} arise from the lattice modes; the modes at 200–400 cm^{-1} correspond to the chains' deformations and the ρr, ρw, and ρτ modes of the VO_2 groups; the mode at 473 cm^{-1} represents the δ(VO_2) mode; the modes at 600–900 cm^{-1} stem from the ν(V–O–V) bonds; and the modes above 900 cm^{-1} stem from the ν(V=O) motions in individual VO_4 tetrahedra.[29,49] Detailed Raman frequency and assignment are shown in Table S2 and Fig. S1. With increasing pressure to 12.5 GPa, new Raman modes are observed in all frequency ranges and accompanied by the disappearance of some strong initial modes, suggesting the occurrence of a structural phase transition. Specifically, several close peaks in 0–200 cm^{-1} gradually merged, and a new mode emerged at 146 cm^{-1}, which should be related to the lattice distortion. The modes at 200–600 cm^{-1} show a more drastic change at 12.5 GPa. All peaks in this range were extremely weakened and almost disappeared, while a new mode at 296 cm^{-1} appeared, indicating a disorder of the initial chain structure. Meanwhile, two prominent peaks at 658 and 956 cm^{-1} appeared in the high-frequency region, further indicating that the V–O–V bonds in the chain skeleton are severely twisted and the VO_4 tetrahedra are distorted. It is worth noting that the 956 cm^{-1} mode splitting from the strongest peak has shown up at ~7 GPa, which corresponds to the emergence of a shoulder peak at 11.3° in the XRD pattern and implies that the VO_4 tetrahedra may start to distort slightly at ~7 GPa, while the chain rearrangement with symmetry conversion is triggered at 12.5 GPa. When the pressure exceeds 12.5 GPa, the Raman peaks significantly weaken with increasing pressure and become almost undetectable at 20.5 GPa. It could be attributed to the structural transition that disrupts the distribution and coherence of the collective Raman modes, thereby leading to a decrease in intensity of the Raman scattering peaks. As a result, we can see that the changes of Raman modes under pressure agree well with the

TABLE I. Experimental lattice parameters at 0 GPa for the *Pbcm* phase and at 15.7 GPa for the *Pc* phase, compared to the reported experimental data [14, 48] at 0 GPa and our calculated data at 16 GPa.

Structure	Method	a (Å)	b (Å)	c (Å)	β (°)	P (GPa)
Pbcm	Expt.	5.458	12.404	5.851	90.00	0.0
	Expt.[14]	5.413	12.291	5.806	90.00	0.0
	Expt.[48]	5.393	12.249	5.786	90.00	0.0
Pc	Expt.	6.084	6.199	5.963	143.92	15.7
	Cal.	7.107	6.088	5.663	144.15	16.0

XRD data and prove the structural transition process of $CsVO_3$ from *Pbcm* to *Pc* symmetry.

C. Optical properties of $CsVO_3$

We next investigated the optical properties of $CsVO_3$ under pressure. Figure 3(a) shows the PL spectra of $CsVO_3$ up to 20.5 GPa excited by a 360 nm laser, and the detailed PL peak positions as a function of pressure are plotted in Fig. 3(b). The ambient PL spectra were found to have a broad emission band with a maximum at ~542 nm. Upon compression, the PL peak position remains almost unchanged at pressures below 6.8 GPa, followed by a successive red shift from 542 nm (6.8 GPa) to 672 nm (13.2 GPa). Afterward, the PL peak exhibits a tiny blue shift with further increasing pressure above 13.2 GPa. Meanwhile, the full-width at half-maximum (FWHM) shows a continuous increase above 6.8 GPa, ranging from 158 nm (6.8 GPa) to 194 nm (above 13.2 GPa). The luminescent colors of $CsVO_3$ under pressure are represented using the Commission internationale de l'éclairage (CIE) chromaticity diagram as shown in Fig. 3(c). The chromaticity coordinate at ambient pressure is located in the yellow-green region (0.3436, 0.4661). As the pressure increases, the CIE coordinates change toward the white region, corresponding to the broadened PL spectra at high pressure. Based on the XRD and Raman results, we can see that the luminescence evolution is quite consistent with the structural transition process. The red shift and broadening of the PL peak starting at 6.8 GPa coincide with the emergence of the high-pressure *Pc* phase. While the redshift and broadening behavior finish at 13.2 GPa, the PL response changes to a white-light emission band, corresponding to the completion of the structural phase transition. It has been demonstrated above that the structural transition from the *Pbcm* to *Pc* phases is accompanied by the distortion of VO_4 tetrahedra. Therefore, the luminescence evolution of $CsVO_3$ can be attributed to the breaking of T_d symmetry in VO_4 tetrahedra.

D. Energy band structure of CsVO3 under pressure

Figure 4(a) shows the ultraviolet–visible (UV–vis) absorption spectra at various pressures up to 20 GPa. A red shift of the absorption edge can be observed upon compression, consistent with the PL measurement results in Fig. 3. From 0.5 to 11.2 GPa, $CsVO_3$ exhibits a sharp absorption edge, corresponding to a direct bandgap semiconductor. With increasing pressure above 12.1 GPa, the absorption spectra change significantly toward a gentle-slope shape, suggesting a direct-indirect bandgap transition.[50] According to the Tauc plot analysis,[51,52] the bandgap width of $CsVO_3$ under different pressures can be obtained by extrapolating the linear region of $(\alpha h\nu)^{1/n}$ vs $h\nu$, as shown in Fig. 4(b) and the insets, where α is the absorption coefficient, $h\nu$ is the photon energy, n is equal to 1/2 for direct bandgap

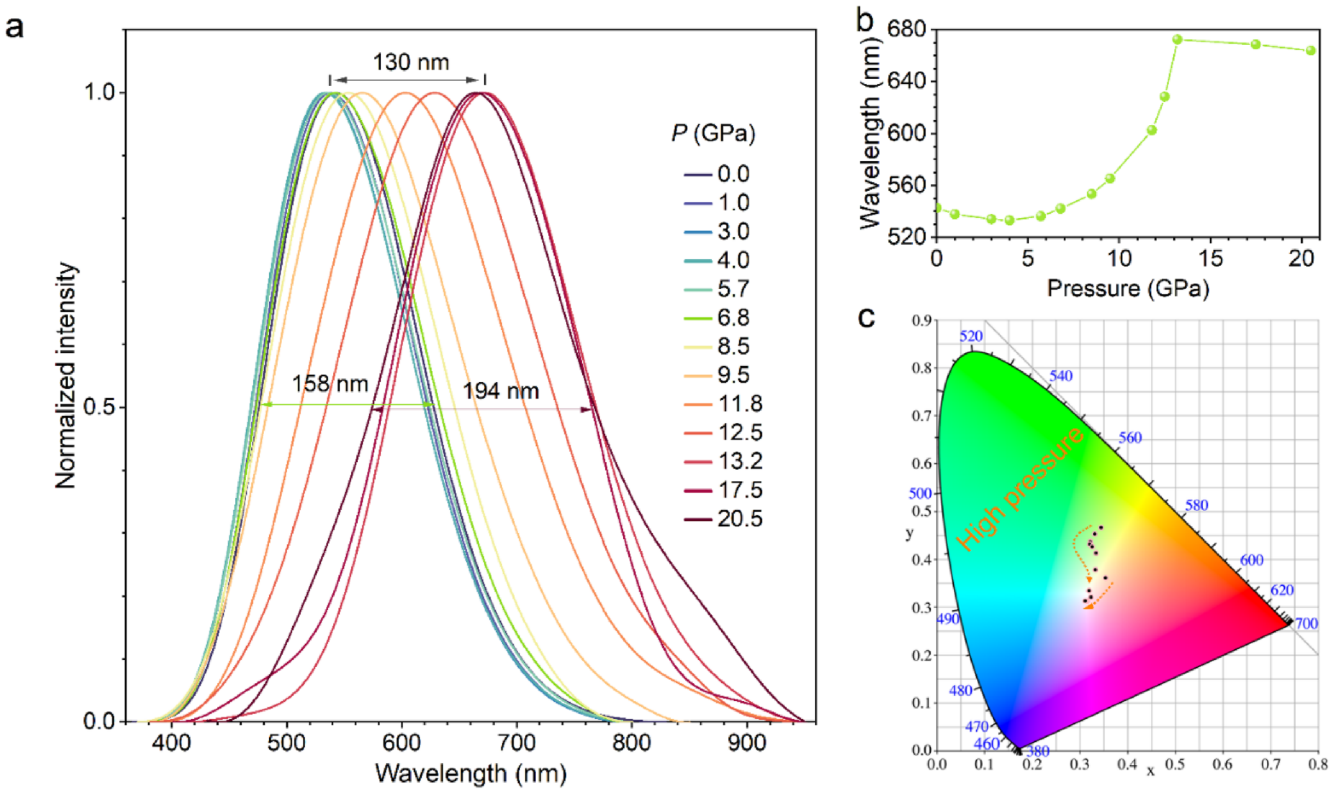

FIG. 3. (a) Pressure-dependent PL spectra of $CsVO_3$ under laser excitation of 360 nm. (b) The emission peak positions of $CsVO_3$ as a function of pressure. (c) CIE chromaticity diagram of $CsVO_3$ at different pressures.

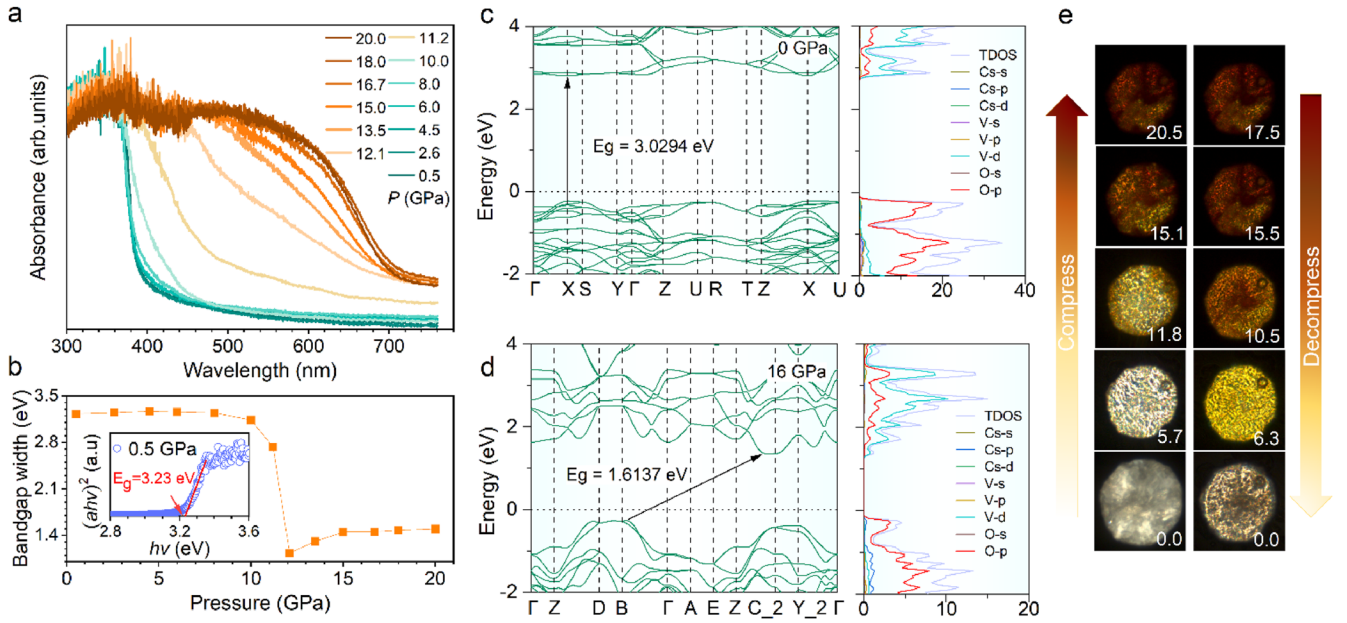

FIG. 4. (a) UV–vis absorption spectra of $CsVO_3$ under pressure. (b) Bandgap energy of $CsVO_3$ estimated from the absorption spectra in the UV region as a function of pressure. (c) and (d) Calculated energy band structures and density of states for the *Pbcm* phase at 0 GPa and for the *Pc* phase at 16 GPa. (e) Optical images of $CsVO_3$ during compression and decompression.

semiconductors and equal to 2 for indirect bandgap semiconductors. At ambient pressure, the direct bandgap width of $CsVO_3$ is estimated to be 3.23 eV, consistent with the previous studies.[13,30] As the pressure increases, the direct bandgap width decreases slightly from 3.23 to 2.73 eV within the pressure range below 11.2 GPa. When the pressure increases to 12 GPa, $CsVO_3$ transforms into an indirect bandgap semiconductor accompanied by a rapid decrease in bandgap width from 2.73 to 1.13 eV, which corresponds to the structural transition from the *Pbcm* to the *Pc* phase. Afterward, the indirect bandgap width gradually increases with further compression up to 20 GPa, suggesting a stabilization of the electronic structure in the high-pressure Pc phase. In addition, a remarkable piezochromic behavior can be observed through the optical micrographs of $CsVO_3$ under pressure, as shown in Fig. 4(e). At ambient pressure, $CsVO_3$ exhibits a pale-yellow body color. As pressure increases, the color gradually changes to orange-red and even to deep red at 15 GPa. Upon decompression, the sample is restored to the initial color with a hysteresis process, indicating that the piezochromism is reversible.

Based on the ambient-pressure *Pbcm* structure and the high-pressure *Pc* structure, we further calculated the energy band structures and density of states (DOS) of $CsVO_3$ at 0 and 16 GPa. The calculation results demonstrate a direct bandgap width of 3.03 eV at 0 GPa and an indirect bandgap width of 1.61 eV at 16 GPa [Figs. 4(c) and 4(d)]. The calculated bandgaps are slightly lower than the experimental values, which is consistent with the known underestimation tendency of the LDA functional. However, the calculations correctly capture the direct-to-indirect transition, confirming the electronic structure modification across the phase transition. On the other hand, the DOS shows that the valence band maximum (VBM) is mainly contributed by the O *2p* electrons, while the conduction band minimum (CBM) is contributed by the V *3d* electrons. The CBM is more susceptible to the phase transition and changes significantly under pressure, so the bandgap width of $CsVO_3$ is mainly dominated by the CBM changes upon compression.

IV. CONCLUSION

In summary, we investigated the crystal structure and optical properties of $CsVO_3$ under pressure up to 20 GPa. Combining *in situ* x-ray diffraction, Raman spectroscopy measurements, and *ab initio* calculations, we identified a pressure-induced structural transition in $CsVO_3$ from the orthorhombic *Pbcm* phase to a monoclinic *Pc* phase at ~12 GPa. The structural transition is accompanied by the distortion and reorientation of VO_4 tetrahedra, resulting in an ultrabroad emission tunability both in peak position (from 542 to 672 nm) and FWHM (from 158 to 194 nm). Absorption spectra and first-principles calculations revealed that $CsVO_3$ also undergoes a direct-indirect bandgap transition at ~12 GPa, corresponding to the structural phase transition. These findings establish the relationship between structural transition and optical properties in $CsVO_3$ and expand our understanding of metavanadate phosphor under pressure.

SUPPLEMENTARY MATERIAL

See the supplementary material for the calculated lattice parameters and atomic coordinates for both the *Pbcm* and *Pc* phases, the Raman spectra, frequencies, and assignment of $CsVO_3$ at ambient pressure.

ACKNOWLEDGMENTS

This study was supported by the National Natural Science Foundation of China (Grant Nos. 12404012, 11774126, T2225013, and 12374010), the Program of China Postdoctoral Science Foundation (Grant No. 2025M773428), the Natural Science Foundation of Jilin Province (Grant No. SKL202302005), the Shanghai Science and Technology Committee (Grant No. 22JC1410300), the Shanghai Key Laboratory of Material Frontiers Research in Extreme Environments (Grant No. 22dz2260800), and the National Key Research and Development Program of China (Grant No. 2022YFA1402304).

AUTHOR DECLARATIONS

Conflict of Interest

The authors have no conflicts to disclose.

Author Contributions

Zhenfang Xing, Yuntao Jie, and Yuqi Sun contributed equally to this study.

Zhenfang Xing: Data curation (equal); Formal analysis (equal); Investigation (equal); Methodology (equal); Visualization (equal); Writing – original draft (equal). **Yuntao Jie**: Data curation (equal); Investigation (supporting); Methodology (equal); Visualization (supporting); Writing – original draft (equal). **Yuqi Sun**: Data curation (equal); Investigation (equal); Methodology (equal); Resources (equal); Visualization (equal); Writing – original draft (equal). **Xingxing Zhao**: Investigation (supporting). **Di Peng**: Data curation (supporting). **Songhao Guo**: Data curation (supporting). **Yifan Zhang**: Data curation (supporting). **Congcong Chen**: Formal analysis (supporting). **Tongge Xu**: Data curation (supporting). **Ziyao Liu**: Data curation (supporting). **Gui Wang**: Data curation (supporting); Formal analysis (supporting). **Xujie Lü**: Resources (equal). **Zhidan Zeng**: Formal analysis (supporting). **Yonghao Han**: Conceptualization (equal); Funding acquisition (equal); Supervision (equal); Visualization (supporting); Writing – review & editing (equal). **Lin Zhao**: Conceptualization (equal); Funding acquisition (equal); Supervision (equal); Visualization (equal); Writing – review & editing (equal). **Meiling Xu**: Funding acquisition (equal); Supervision (equal); Validation (supporting). **Qiaoshi Zeng**: Funding acquisition (equal); Supervision (equal).

DATA AVAILABILITY

The data that support the findings of this study are available from the corresponding authors upon reasonable request.

REFERENCES

[1] H. Gobrecht and G. Heinsohn, Z. Phys. **147**, 350 (1957).
[2] B. V. Slobodin, A. V. Ishchenko, R. F. Samigullina, O. S. Teslenko, B. V. Shul'gin, and D. Yu. Zhurakovskii, Inorg. Mater. **47**(10), 1126 (2011).
[3] R. K. Sharme, M. R. Islam, M. A. Sarker, M. Solayman, M. Al Momin, and M. R. Islam, Physica B **681**, 415785 (2024).
[4] T. Nakajima, M. Isobe, T. Tsuchiya, Y. Ueda, and T. Kumagai, Nat. Mater. **7**(9), 735 (2008).
[5] G. S. R. Raju, G. L. Varaprasad, J. H. Lee, J. Y. Park, N. R. Chodankar, K. S. Ranjith, E. Pavitra, Y. S. Huh, and Y. K. Han, Nanomaterials **12**(16), 2864 (2022).
[6] S. Shisina, K. G. Nishanth, and S. Das, Inorg. Chem. **64**(11), 5386 (2025).
[7] Y. Ma, G. Sun, X. Meng, K. Shi, C. Ge, D. Wu, S. Ji, and X. Cao, Ceram. Int. **51**(15), 21102 (2025).
[8] Y. Dong, Z. Liu, S. Yang, B. Shao, Q. Zhu, and C. Wang, Ceram. Int. **50**(18), 32947–32953 (2024).
[9] H. Miyazaki and Y. Mimaru, Opt. Mater. **114**, 111004 (2021).
[10] T. Matsuura, H. Miyazaki, and T. Ota, J. Ceram. Soc. Jpn. **125**(8), 657 (2017).
[11] G. Sun, W. Li, S. Ji, X. Cao, and P. Jin, Res. Chem. Intermed. **43**(1), 341 (2017).
[12] T. Nakajima, K. Shinoda, and T. Tsuchiya, RSC Adv. **4**(37), 19165 (2014).
[13] F. El Mellouhi, A. Akande, C. Motta, S. N. Rashkeev, G. Berdiyorov, M. E. A. Madjet, A. Marzouk, E. T. Bentria, S. Sanvito, S. Kais, and F. H. Alharbi, ChemSusChem **10**(9), 1931 (2017).
[14] E. Pavitra, G. S. R. Raju, L. K. Bharat, J. Y. Park, C. H. Kwak, J. W. Chung, Y. K. Han, and Y. S. Huh, J. Mater. Chem. C **6**(46), 12746 (2018).
[15] M. Sayer, Phys. Status Solidi **1**(2), 269 (1970).
[16] T. Nakajima, M. Isobe, Y. Uzawa, and T. Tsuchiya, J. Mater. Chem. C **3**(41), 10748 (2015).
[17] X. Qiao, Y. Li, Y. Wan, Y. Huang, H. Cheng, and H. J. Seo, J. Alloys Compd. **656**, 843 (2016).
[18] H. Ronde and G. Blasse, J. Inorg. Nucl. Chem. **40**(2), 215 (1978).
[19] J. V. Tol, J. A. V. Hulst, and J. H. V. D. Waals, Mol. Phys. **76**, 547 (1992).
[20] J. V. Tol and J. H. V. D. Waals, Mol. Phys. **76**(3), 567 (1992).
[21] A. V. Ishchenko, K. V. Ivanovskikh, I. A. Weinstein, R. F. Samigullina, and V. V. Platonov, Radiat. Meas. **124**, 48 (2019).
[22] T. Nakajima, M. Isobe, T. Tsuchiya, Y. Ueda, and T. Manabe, Opt. Mater. **32**(12), 1618 (2010).
[23] T. Nakajima, M. Isobe, T. Tsuchiya, Y. Ueda, and T. Manabe, J. Phys. Chem. C **114**(11), 5160 (2010).
[24] T. Nakajima, M. Isobe, T. Tsuchiya, Y. Ueda, and T. Kumagai, J. Lumin. **129**(12), 1598 (2009).
[25] W. Zhao, G. Xiao, S. Qiu, Y. Shang, Y. Qin, J. Yang, J. Wang, J. Ning, Y. Fang, Q. Dong, Z. Liu, S. Li, J. Gao, and B. Zou, Angew. Chem., Int. Ed. **64**(23), e202504913 (2025).
[26] Z. Li, Q. Li, H. Li, L. Yue, D. Zhao, F. Tian, Q. Dong, X. Zhang, X. Jin, L. Zhang, R. Liu, and B. Liu, Adv. Funct. Mater. **32**(8), 2108636 (2022).
[27] S. Guo, Y. Zhao, K. Bu, Y. Fu, H. Luo, M. Chen, M. P. Hautzinger, Y. Wang, S. Jin, W. Yang, and X. Lü, Angew. Chem., Int. Ed. **59**(40), 17533 (2020).
[28] D. M. Adams, A. G. Christy, J. Haines, and S. Leonard, J. Phys.: Condens. Matter **3**(32), 6135 (1991).
[29] G. A. Kourouklis, A. Jayaraman, G. P. Espinosa, and A. S. Cooper, J. Raman Spectrosc. **22**(2), 57 (1991).
[30] S. S. Essaoud, A. Bouhemadou, S. Maabed, S. B. Omran, and R. Khenata, Philos. Mag. **102**(15), 1522 (2022).
[31] J. Luo, A. Yang, Z. Xie, J. Huang, and X. Zuo, J. Lumin. **229**, 117658 (2021).
[32] J. Luo, A. Yang, X. Wang, and K. Liu, Ferroelectrics **564**(1), 52 (2020).
[33] H. K. Mao, J. Xu, and P. M. Bell, J. Geophys. Res.: Solid Earth **91**(B5), 4673, https://doi.org/10.1029/jb091ib05p04673 (1986).
[34] C. Prescher and V. B. Prakapenka, High Pressure Res. **35**(3), 223 (2015).
[35] H. M. Retveld, J. Appl. Cryst. **2**(2), 65 (1969).
[36] Y. Wang, J. Lv, L. Zhu, and Y. Ma, Phys. Rev. B **82**(9), 094116 (2010).
[37] Y. Wang, J. Lv, L. Zhu, and Y. Ma, Comput. Phys. Commun. **183**(10), 2063 (2012).
[38] Y. Wang and Y. Ma, J. Chem. Phys. **140**(4), 040901 (2014).
[39] B. Gao, P. Gao, S. Lu, J. Lv, Y. Wang, and Y. Ma, Sci. Bull. **64**(5), 301 (2019).
[40] X. Shao, J. Lv, P. Liu, S. Shao, P. Gao, H. Liu, Y. Wang, and Y. Ma, J. Chem. Phys. **156**(1), 014105 (2022).
[41] W. Kohn and L. J. Sham, Phys. Rev. **140**(4A), A1133 (1965).
[42] G. Kresse and J. Hafner, Phys. Rev. B **48**(17), 13115 (1993).
[43] G. Kresse and J. Furthmüller, Phys. Rev. B **54**(16), 11169 (1996).
[44] M. Jex, M. Lewin, and P. S. Madsen, Rev. Math. Phys. **37**(04), 2450037 (2025).
[45] P. E. Blöchl, Phys. Rev. B **50**(24), 17953 (1994).

[46]H. J. Monkhorst and J. D. Pack, Phys. Rev. B **13**(12), 5188 (1976).
[47]A. Togo, F. Oba, and I. Tanaka, Phys. Rev. B **78**(13), 134106 (2008).
[48]F. C. Hawthorne and C. Calvo, J. Solid State Chem. **22**(2), 157 (1977).
[49]D. M. Adams and P. A. Fletcher, Spectrochim. Acta, Part A **44**(2), 233 (1988).
[50]J. Gong, H. Zhong, C. Gao, J. Peng, X. Liu, Q. Lin, G. Fang, S. Yuan, Z. Zhang, and X. Xiao, Adv. Sci. **9**, 2201554 (2022).
[51]J. Tauc, R. Grigorovici, and A. Vancu, Phys. Status Solidi B **15**(2), 627–637 (1966).
[52]P. Makuła, M. Pacia, and W. Macyk, J. Phys. Chem. Lett. **9**(29), 6814 (2018).